Article

Magnetic sensitivity of cryptochrome 4 from a migratory songbird

https://doi.org/10.1038/s41586-021-03618-9

Received: 17 July 2019

Accepted: 6 May 2021

Published online: 23 June 2021

Check for updates

Jingjing Xu[1], Lauren E. Jarocha[2], Tilo Zollitsch[2], Marcin Konowalczyk[3], Kevin B. Henbest[2,3], Sabine Richert[4], Matthew J. Golesworthy[3], Jessica Schmidt[1], Victoire Déjean[3], Daniel J. C. Sowood[2], Marco Bassetto[1,2], Jiate Luo[2], Jessica R. Walton[2], Jessica Fleming[2], Yujing Wei[2], Tommy L. Pitcher[3], Gabriel Moise[3], Maike Herrmann[1], Hang Yin[5], Haijia Wu[6], Rabea Bartölke[1], Stefanie J. Käsehagen[1], Simon Horst[1], Glen Dautaj[1], Patrick D. F. Murton[2], Angela S. Gehrckens[2], Yogarany Chelliah[7,8], Joseph S. Takahashi[7,8], Karl-Wilhelm Koch[6,9], Stefan Weber[4], Ilia A. Solov'yov[9,10]✉, Can Xie[11,12]✉, Stuart R. Mackenzie[2]✉, Christiane R. Timmel[3,13]✉, Henrik Mouritsen[1,9]✉ & P. J. Hore[2]✉

Night-migratory songbirds are remarkably proficient navigators[1]. Flying alone and often over great distances, they use various directional cues including, crucially, a light-dependent magnetic compass[2,3]. The mechanism of this compass has been suggested to rely on the quantum spin dynamics of photoinduced radical pairs in cryptochrome flavoproteins located in the retinas of the birds[4–7]. Here we show that the photochemistry of cryptochrome 4 (CRY4) from the night-migratory European robin (*Erithacus rubecula*) is magnetically sensitive in vitro, and more so than CRY4 from two non-migratory bird species, chicken (*Gallus gallus*) and pigeon (*Columba livia*). Site-specific mutations of *Er*CRY4 reveal the roles of four successive flavin–tryptophan radical pairs in generating magnetic field effects and in stabilizing potential signalling states in a way that could enable sensing and signalling functions to be independently optimized in night-migratory birds.

The radical-pair mechanism is a well-established source of magnetic field effects on the rates and yields of chemical reactions[8]. Proof-of-principle experiments have demonstrated the sensitivity of a model radical-pair system to the direction of an Earth-strength magnetic field (around 50 μT) via magnetic interactions that are a million times smaller than the thermal energy[9,10], k_BT (in which k_B is the Boltzmann constant and T is temperature). [$FAD^{\bullet-}$ $TrpH^{\bullet+}$] radical pairs in cryptochromes are formed by the sequential hopping of an electron along a chain of three or four tryptophans to the photoexcited, non-covalently bound flavin adenine dinucleotide (FAD) chromophore[11–15]. Magnetically sensitive, light-induced radical pairs have been reported in vitro for a few members of the cryptochrome/photolyase family of proteins: *At*CRY1 (*Arabidopsis thaliana*), *Dm*Cry (*Drosophila melanogaster*) and *Escherichia coli* photolyase[16,17]. Indeed, a generic sensitivity of cryptochromes to magnetic fields would be required to provide evolution with scope for species-specific optimization in animals in which an awareness of the Earth's magnetic field would be advantageous for survival and fitness. The detailed properties of cryptochromes from non-migratory species such as plants and fruit flies[18–23] might therefore not be relevant when considering magnetoreception in long-distance, night-migratory passerine birds. So far, no cryptochrome from a migratory animal that unequivocally uses a light-dependent magnetic compass has been shown to exhibit magnetic sensitivity.

Magnetic field effects on the coherent spin dynamics of light-induced radical pairs in cryptochromes are manifested as changes in the quantum yields of stabilized states of the protein that could initiate magnetic signalling, most probably through a change in the conformation of the C-terminal tail[24]. Here we present a detailed in vitro analysis of the photochemistry and magnetic sensitivity of *Er*CRY4, a protein that is expressed in double-cone and long-wavelength single-cone photoreceptor cells in the eyes of night-migratory European robins[25]. In addition to the light-induced radical pairs studied here, it has been suggested that radical pairs formed by 'dark' back-reactions could also be responsible for the magnetic sensitivity of cryptochromes in vivo and that CRY1a could be more suitable as a magnetoreceptor than CRY4[21,26–30] (but see ref. [31]). However, the identity of any 'dark' radical pairs is unknown, and vertebrate CRY1a proteins seem not to bind FAD strongly in vitro[29,32]. We have therefore focused our investigation on whether light-induced electron-transfer reactions in *Er*CRY4 in vitro are fit for purpose for magnetic sensing.

[1]AG Neurosensory Sciences/Animal Navigation, Institut für Biologie und Umweltwissenschaften, Carl-von-Ossietzky Universität Oldenburg, Oldenburg, Germany. [2]Physical and Theoretical Chemistry Laboratory, Department of Chemistry, University of Oxford, Oxford, UK. [3]Inorganic Chemistry Laboratory, Department of Chemistry, University of Oxford, Oxford, UK. [4]Institut für Physikalische Chemie, Albert-Ludwigs-Universität Freiburg, Freiburg, Germany. [5]Department of Medicinal Chemistry and Molecular Pharmacology, Purdue University, West Lafayette, IN, USA. [6]Division of Biochemistry, Department of Neuroscience, Carl-von-Ossietzky-Universität Oldenburg, Oldenburg, Germany. [7]Department of Neuroscience, University of Texas Southwestern Medical Center, Dallas, TX, USA. [8]Howard Hughes Medical Institute, University of Texas Southwestern Medical Center, Dallas, TX, USA. [9]Research Centre for Neurosensory Science, University of Oldenburg, Oldenburg, Germany. [10]Department of Physics, Carl-von-Ossietzky Universität Oldenburg, Oldenburg, Germany. [11]High Magnetic Field Laboratory, Key Laboratory of High Magnetic Field and Ion Beam Physical Biology, Hefei Institutes of Physical Science, Chinese Academy of Sciences, Hefei, PR China. [12]International Magnetobiology Frontier Research Center, Hefei, PR China. [13]Centre for Advanced Electron Spin Resonance (CAESR), Department of Chemistry, University of Oxford, Oxford, UK. ✉e-mail: ilia.solovyov@uni-oldenburg.de; canxie@hmfl.ac.cn; stuart.mackenzie@chem.ox.ac.uk; christiane.timmel@chem.ox.ac.uk; henrik.mouritsen@uni-oldenburg.de; peter.hore@chem.ox.ac.uk

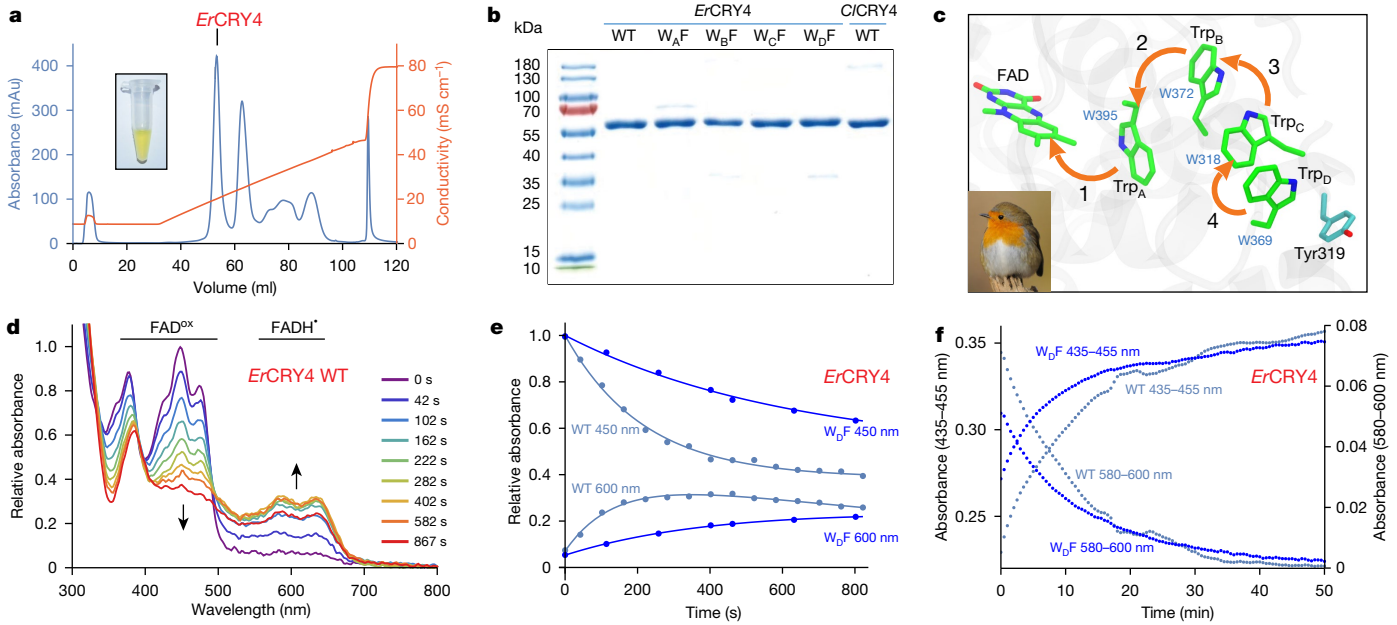

Fig. 1 | Purification, electron transfer pathway and photoreduction of European robin CRY4. a, Purification of wild-type *Er*CRY4 by anion-exchange chromatography. The protein fractions in the first peak of the gradient elution contained yellow *Er*CRY4 with FAD bound. **b**, Verification of protein purity by SDS–PAGE Coomassie blue staining: wild-type (WT) and Trp_X-to-Phe (X = A–D) mutants of *Er*CRY4, and wild-type *Cl*CRY4. **c**, Structural homology model of *Er*CRY4 showing the flavin group of the FAD chromophore, the Trp-tetrad and Tyr 319. Sequential electron transfers are indicated by arrows. Robin photograph by Thomas Eisenhut (© www.xeta.at). **d**, Photoreduction of wild-type *Er*CRY4 by continuous irradiation at 450 nm. UV–visible absorption spectra show depletion of FAD^{ox} (<500 nm) and accumulation of $FADH^{\bullet}$ (550–650 nm). The shoulders at around 480 nm on the peak at 450 nm are characteristic of correctly bound FAD^{ox}. **e**, Time dependence of FAD^{ox} depletion (450 nm) and $FADH^{\bullet}$ formation (600 nm). The faster photoreduction kinetics seen for the wild-type protein are consistent with a greater stabilization of photoinduced radicals than in the W_DF mutant. The decrease in radical absorbance (600 nm) for the wild-type after 500 s illumination arises from photoreduction of $FADH^{\bullet}$ to $FADH^-$. **f**, Time-dependence of the oxidation of $FADH^{\bullet}$ (580–600 nm) and the recovery of FAD^{ox} (435–455 nm) under aerobic conditions after a 2-min period of illumination at 450 nm. No oxidizing or reducing agents were added to the samples. Note the different vertical scales for the two wavelength bands. See Supplementary Figs. 15–17 and Supplementary Table 5 for further details. See Supplementary Methods for experimental details.

To characterize its photochemistry and magnetic properties, we recombinantly expressed and purified[33] wild-type *Er*CRY4 as a yellow protein containing the fully oxidized chromophore, FAD^{ox}, which is essential for radical pair formation[4] (Fig. 1a, b). Optical spectroscopy (Fig. 1d) and mass spectrometry (Supplementary Fig. 13) experiments confirmed the incorporation of FAD^{ox} (greater than 97%). *Er*CRY4 contains a chain of four tryptophan residues stretching from the FAD to the surface of the protein[25] (Fig. 1c). To determine the roles of these residues in radical-pair production, we also prepared site-specific mutants of *Er*CRY4 by replacing each of the tryptophans with a redox-inactive phenylalanine: W395F, W372F, W318F and W369F (Fig. 1b). We refer to these four residues as Trp_X (X = A, B, C or D, respectively) and to the corresponding mutants as W_XF. RP_X denotes the radical pair, [$FAD^{\bullet-}$ $Trp_XH^{\bullet+}$], containing the protonated cation radical form of Trp_X. All the mutated *Er*CRY4 forms bind FAD^{ox} (Supplementary Fig. 1).

We have developed and continuously refined several spectroscopic techniques specifically to study magnetic field effects on cryptochrome photochemistry. Cavity ring-down spectroscopy (CRDS)[34] and broadband cavity-enhanced absorption spectroscopy[35] both take advantage of the huge optical path lengths that are achievable by multiple passes of the probe light through a sample placed between highly reflective mirrors. Higher time-resolution was provided by a conventional single-pass transient absorption spectrometer equipped with magnetic field coils.

Transient absorption measurements were used to investigate the formation and stabilization of light-induced radicals. Laser excitation (at 450 nm) of W_BF, W_CF, W_DF and wild-type *Er*CRY4 reduced FAD^{ox} ground-state absorption and produced signals that are characteristic of $FAD^{\bullet-}$ and $TrpH^{\bullet+}$ radicals with lifetimes that steadily increase (around 200 ps, around 1 ns, greater than 1 µs and greater than 1 µs, respectively) as the electron transfer chain is extended and as charge recombination (that is, the return to the ground state: [$FAD^{\bullet-}$ $Trp_XH^{\bullet+}$] → FAD^{ox} + Trp_XH) becomes less efficient (Supplementary Fig. 2). No radicals were observed for W_AF, which lacks the tryptophan nearest the FAD; this implies the absence of an alternative electron donor that is capable of reducing the FAD and forming radical pairs with lifetimes longer than around 100 ps. Unlike W_BF and W_CF, the radical pairs formed in both W_DF and in wild-type *Er*CRY4 are sufficiently long-lived that they could be sensitive to the geomagnetic field.

Continuous blue-light illumination of both wild-type *Er*CRY4 and *Er*CRY4 W_DF resulted in the reduction of FAD^{ox} to the neutral semiquinone radical, $FADH^{\bullet}$ (Fig. 1d); this confirms the existence of an intramolecular electron transfer pathway and the stabilization of $FAD^{\bullet-}$ by protonation to form $FADH^{\bullet}$ in both proteins on a timescale (greater than 10 µs) that is beyond the range of the transient absorption measurements. Wild-type *Er*CRY4 is more easily photoreduced than is W_DF (Fig. 1e).

Figure 2a shows the effect of an applied magnetic field on the absorbance of FAD and Trp radicals in wild-type *Er*CRY4, measured by CRDS 2 µs after photoexcitation (450 nm) at 5 °C. Millitesla fields suppress radical yields by favouring return to the ground state, as expected for radical pairs that are formed in a spin-correlated singlet state[17]. Under physiological conditions (40–43 °C), the pH of most bird cells[36,37] is 7.3. The change in the charge states of proteins caused by a reduction in temperature—principally due to a shift in the acid–base equilibrium of histidine side chains—can be reversed by an increase in pH (Supplementary Information), which suggests that a pH of approximately 8 at 5 °C should be equivalent to physiological conditions (pH 7.3 at

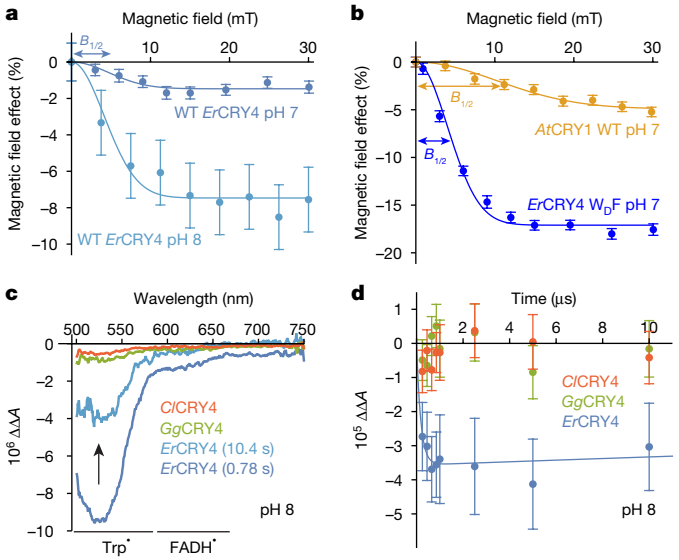

Fig. 2 | Magnetic field effects on the yields of photoinduced radicals in CRY4 proteins. a, **b**, Magnetic field effect (percentage change in absorbance induced by the magnetic field) on the optical absorbance of photoinduced radicals 2 μs after a 450-nm laser pulse in wild-type *Er*CRY4 at pH 7 and pH 8 (**a**) and in W_DF and in wild-type *At*CRY1 at pH 7 (**b**). Data were measured by CRDS at 530 nm. The smaller value of $B_{1/2}$ (the magnetic field that produces 50% of the limiting change seen at high field) for wild-type *Er*CRY4 (4.9 ± 1.6 mT) compared to wild-type *At*CRY1 (14.3 ± 1.7 mT) suggests that, other factors being equal, the former would be more sensitive to weak magnetic fields. **c**, Change in the optical absorbance of photoinduced radicals in three avian CRY4 samples induced by a 30-mT magnetic field. All four broadband cavity-enhanced absorption spectra measured using continuous illumination at 450 nm are dominated by the field-induced reduction in the yield of $Trp^•$ radicals, which absorb in the 500–600 nm range. *Er*CRY4 spectra are shown at two different times after the start of illumination. The equivalent spectra of *Cl*CRY4 and *Gg*CRY4 showed no time dependence and are averages over the first 9 s. The weak signals at wavelengths greater than 600 nm are thought to arise from magnetic field effects on the formation of $FADH^•$. **d**, Change in the photoinduced optical absorbance of three avian CRY4 samples upon application of a 30 mT magnetic field, measured by CRDS at 530 nm. Within error, the magnetic field effects on the CRY4 proteins from the non-migratory pigeon and chicken could not be distinguished from zero (apart from one very early data point for *Cl*CRY4). See Supplementary Methods for experimental details and statistical information. Data in **a**, **b**, **d** are mean ± s.e.m.

40–43 °C)[36,37]. It may be relevant, therefore, that the magnetic field effect on wild-type *Er*CRY4 at 5 °C is substantially larger at pH 8 than at pH 7 (Fig. 2a).

If the magnetic field effect on CRY4 forms the basis of the magnetic compass sense in night-migratory robins, it should have been optimized by evolution. We therefore compared the magnetic field effects on *Er*CRY4 with those on CRY4 proteins from two non-migratory birds, pigeon[33] (*C. livia*) and chicken (*G. gallus*), in which we expect there to have been less evolutionary pressure to optimize any light-dependent magnetic compass sense. Figure 2c shows the change in the optical absorption spectra of the three proteins caused by a 30-mT magnetic field under conditions of continuous illumination at 450 nm. The band between 500 nm and 550 nm suggests a considerably bigger magnetic field effect on the yield of neutral $Trp^•$ radicals in *Er*CRY4 than in *Cl*CRY4 or *Gg*CRY4. This difference between the three proteins was supported by CRDS (Fig. 2d) by measuring the effect of a 30-mT magnetic field on the radical absorption signal as a function of time after irradiation with blue light. The field produces a significant reduction in the yield of radicals in *Er*CRY4 that persists for more than 10 μs. Apart from one of the earliest data points for *Cl*CRY4, no such change could be observed above the noise level for either *Cl*CRY4 or *Gg*CRY4. Taking the results of the two experiments together, the magnetic sensitivity of CRY4 from the night-migratory robin is substantially larger than that of the CRY4 proteins from the non-migratory—primarily diurnal—pigeon and chicken.

For a molecule to act as a receptor, it must switch on in response to a stimulus and either switch off again by returning to its resting state or be replaced by freshly expressed protein. For *Er*CRY4, it would therefore be advantageous if the $FADH^•$ and/or $FADH^-$ states were to be oxidized back to the FAD^{ox} state in minutes (rather than hours) in vivo. Illumination of *Er*CRY4—in a cuvette in contact with air and without added oxidants, and at an intensity approximately equivalent to that of sunlight—produced a steady state in which the proportions of the *Er*CRY4 oxidation states were approximately 50% FAD^{ox} and approximately 50% $FADH^•$. When the light was turned off, the recycling times from $FADH^•$ to FAD^{ox} and from $FADH^-$ to $FADH^•$ were around 13 min and around 1 min, respectively (Fig. 1f, Supplementary Information, Supplementary Figs. 15–17, Supplementary Table 5). The re-oxidation times for *Cl*CRY4 and *Gg*CRY4 have similar values (Supplementary Information, Supplementary Table 5). Re-oxidation of *Er*CRY4 in the presence of 5 mM dithiothreitol is slower: about 5 h at 25 °C and about 1 h at the physiological temperature of 40 °C (Supplementary Information, Supplementary Fig. 13, Supplementary Table 6). Although re-oxidation could be slower or faster in vivo, these measurements show that there are conditions under which *Er*CRY4 could cycle fast enough to act as a magnetoreceptor.

The slower photoreduction of W_DF compared to the wild-type protein (Fig. 1e) suggests that Trp_D participates in the formation of radical pairs in wild-type *Er*CRY4 in vitro (as it does in *Dm*Cry[13,14]) by prolonging the lifetime of photoreduced states of the protein. To determine whether the electron-transfer chain in wild-type *Er*CRY4 stops at Trp_C or extends to include Trp_D, we performed time-resolved electron paramagnetic resonance and out-of-phase electron spin echo envelope modulation experiments on wild-type *Er*CRY4 and its W_DF mutant. Both the spin polarization of the time-resolved electron paramagnetic resonance spectra[38] (Fig. 3a) and the existence of an 'out of phase' (that is, 90°-phase-shifted) spin echo[13] (Fig. 3b) confirm the rapid (within 100 ns) formation of singlet radical pairs possessing the non-equilibrium spin-polarization that is a necessary—but not sufficient—condition for magnetic sensitivity. In the latter measurement, the modulation frequencies arise mainly from the electron dipolar coupling, which depends on the centre-to-centre radical separation, r, as r^{-3}. The clearly different modulation frequencies in Fig. 3b are consistent with r being approximately 0.3-nm larger for the wild-type protein than for the mutant (Supplementary Fig. 4). Molecular dynamics simulations predict r = 2.2 nm for RP_D and 1.8 nm for RP_C, and the X-ray structure of *Cl*CRY4 reveals FAD–Trp_D and FAD–Trp_C distances of 2.13 nm and 1.76 nm, respectively[15] (Supplementary Figs. 4, 8, Supplementary Table 2), both of which are consistent with the involvement of Trp_D in electron transport in wild-type *Er*CRY4. Very similar results have recently been reported[39] for pigeon CRY4. The electron paramagnetic resonance spectra of the two proteins bear a strong resemblance to those of the FAD–Trp radical pairs in *Dm*Cry[14], in which the differences in the spectral shapes were related to the larger dipolar coupling in RP_C and the different side-chain orientations of Trp_C and Trp_D radicals. In summary, electron paramagnetic resonance spectroscopy provides strong evidence that photoinduced electron transfer in wild-type *Er*CRY4 results in the formation of [$FAD^{•-}$ $Trp_DH^{•+}$] in a singlet state.

Having established that the electron transfer pathway in wild-type *Er*CRY4 extends as far as Trp_D, it is important to know the role of RP_D in generating the magnetic responses of the protein. Figure 2b shows the magnetic field effects on radical yields in two proteins, *Er*CRY4 W_DF and *At*CRY1, that have a Trp triad and therefore only RP_C. Both are more sensitive to magnetic fields than is wild-type *Er*CRY4 (Fig. 2a) at pH 7. This would seem to be consistent with the 0.3-nm-larger separation

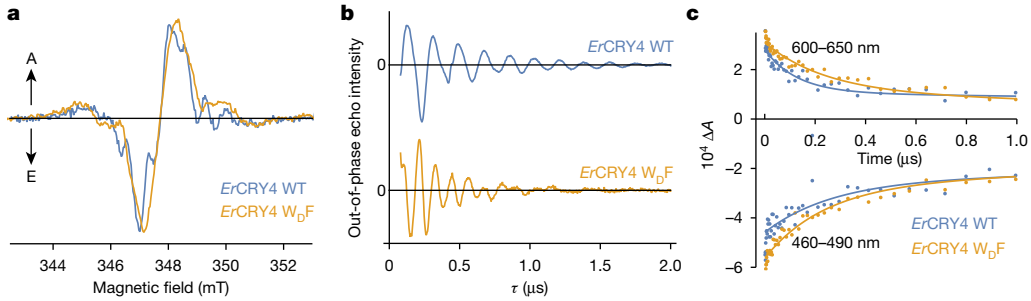

Fig. 3 | Electron paramagnetic resonance and optical spectroscopy of photoinduced FAD–Trp radical pairs in *Er*CRY4. a, Time-resolved X-band (9.75 GHz) electron paramagnetic resonance spectra of wild-type *Er*CRY4 and its W_DF mutant recorded at 1 °C, 0.5 μs after a 450-nm laser pulse. The spectra have been normalized to the same absolute intensity. A, absorptive contribution; E, emissive contribution. **b**, Out-of-phase electron spin echo envelope modulation signals recorded at Q-band frequencies (34 GHz) at 80 K. τ is the interval between the microwave pulses in the spin echo pulse sequence. Slight irregularities in the oscillations could arise from nuclear electron spin echo envelope modulations. **c**, Time dependence of the decay of the transient radical absorption at 600–650 nm and the recovery of the ground state absorption at 460–490 nm for the wild-type and W_DF forms of *Er*CRY4. The lines are guides for the eye. See also Supplementary Fig. 12. See Supplementary Methods section for experimental details.

between the radicals in RP_D, which should make radical recombination much slower than for RP_C[12]. However, we found that the light-induced radicals formed in the two proteins have very similar decay kinetics during the period (up to around 1 μs) in which the magnetic field effects are generated. As shown in Fig. 3c, in both proteins a substantial fraction of the radicals disappears and the ground state recovers with time constants on the order of 100 ns.

To gain further insight, we performed molecular dynamics simulations for five redox states of *Er*CRY4—the diamagnetic ground state and the four radical-pair states, RP_X (X = A, B, C or D)—to obtain order-of-magnitude estimates of the rate constants for electron transfer along the tryptophan chain (Supplementary Table 3, Supplementary Figs. 9, 10). The first two steps, $RP_A \rightarrow RP_B$ and $RP_B \rightarrow RP_C$, are exergonic, fast (>10^{10} s^{-1}) and outpace the reverse reactions ($RP_A \leftarrow RP_B$ and $RP_B \leftarrow RP_C$) by factors of more than 10^4. However, the third electron transfer ($RP_C \leftrightarrow RP_D$), is predicted to have similar forward (k_{CD}) and backward (k_{DC}) rate constants of around 10^{10} s^{-1} (Fig. 4a). The molecular dynamics simulations also provided estimates of the rate constants for the recombination of RP_C and RP_D directly to the ground state, confirming that the former should be one to two orders of magnitude faster than the latter (Fig. 4a, Supplementary Table 3). These rate constants, and those of the other relevant processes (singlet–triplet interconversion and radical (de)protonation), are so much slower than 10^{10} s^{-1} that the RP_C and RP_D states of *Er*CRY4 could be in dynamic equilibrium. The consequence would be a 'composite' radical pair, the spin dynamics and reaction rates of which are weighted averages of the properties of RP_C and RP_D, with the weights given by the fractional populations of the two states, f_C and f_D, where $f_C/f_D = k_{DC}/k_{CD}$. A reaction scheme including this possibility, and showing various estimates of the relevant rate constants, is provided in Fig. 4a. As detailed in the Supplementary Information, the difference in the dipolar couplings measured for wild-type *Er*CRY4 and for W_DF would not be inconsistent with a composite radical pair, provided that the proportion of RP_C at equilibrium is no larger than about 10% (that is, $f_C \leq 0.1$).

To explore whether a rapid equilibrium between the RP_C and RP_D states of wild-type *Er*CRY4 could account for both its smaller magnetic field effect (Fig. 3a) and the kinetic similarity to W_DF (Fig. 3c), we used spin dynamics simulations to calculate the magnetic field effect (Fig. 4b) as a function of the weighted average reaction rate constants, $\langle k_r \rangle$ (return of the singlet pairs to the ground state) and $\langle k_f \rangle$ (the competing forward reaction). Strong magnetic sensitivity requires that these reactions proceed at similar rates, are not too slow to compete with spin relaxation, and are not so fast that there is little time for singlet–triplet interconversion. For $\langle k_f \rangle$ in the range 10^5–10^8 s^{-1}, the maximum magnetic field effect occurs when $\langle k_r \rangle \approx 3\langle k_f \rangle$. Figure 4b shows the combinations of $\langle k_r \rangle$ and $\langle k_f \rangle$ for which the radical pair lifetime is approximately 100 ns (white line) and the points on that line (white spots) that correspond to pure RP_C ($f_C = 1.0$), and a composite radical pair with $f_C = 0.1$. The values of the individual rate constants that underlie these average rate constants are given in the Supplementary Information. The magnetic sensitivity for $f_C = 1.0$ (modelling W_DF) is considerably larger than that for $f_C = 0.1$ (modelling the wild-type protein) because $\langle k_r \rangle$ and $\langle k_f \rangle$ for the latter are far from the 1:3 ratio that is required for a strong magnetic response.

In vivo, a cryptochrome magnetoreceptor would need to be capable of sensing and signalling. The sensing state cannot survive for more than a few microseconds, otherwise any magnetic field effect on the singlet–triplet interconversion would be lost by spin relaxation[40]. However, to trigger a biochemical signalling cascade, a lifetime of milliseconds, seconds or longer is required. No single state of the protein could fulfil both roles. Evolutionary optimization of these functions might be favoured by a composite *Er*CRY4 radical pair formed rapidly in high yield, with inter-radical spin interactions that are not so large that they block singlet–triplet mixing[41] and, as shown by the W_DF mutant, an RP_C component that is capable of generating strong magnetic field effects. The RP_D component, with its larger radical separation, is better placed to generate the signalling state. Being closer to the surface of the protein, $Trp_DH^{\bullet+}$ could deprotonate more efficiently than could $Trp_CH^{\bullet+}$. Alternatively, $Trp_DH^{\bullet+}$ could be stabilized by receipt of an electron from an external reductant or, possibly, from Tyr319[11] (which is only 0.37 nm away[15,25]) (Fig. 1c). On a similar (greater than 1 μs) timescale, $FAD^{\bullet-}$ would become protonated (Figs. 1d, 2c), which would produce the $FADH^{\bullet}$ form of the protein as a potential signalling state (Fig. 4a).

To be sensitive to the Earth's magnetic field (around 50 μT) in vivo, a composite radical pair would need a minimum lifetime[4] of around 1 μs—that is, an order of magnitude longer than the approximately 100-ns lifetime that is observed here for purified wild-type *Er*CRY4 in vitro. Figure 4c shows a simulation performed under identical conditions to those in Fig. 4b except that the magnetic field was 50 μT instead of 30 mT. The maximum magnetic field effect (which occurs when $\langle k_f \rangle \approx 8 \times 10^5$ s^{-1}, $\langle k_r \rangle \approx 2 \times 10^6$ s^{-1}) is smaller than at 30 mT, has opposite phase (the 'low field effect'[42]), and is shifted to lower values of $\langle k_r \rangle$ and $\langle k_f \rangle$, reflecting the smaller electron Larmor frequency in the weaker magnetic field. Superimposed on the contour plot is the locus of rate constants for which the radical pair lifetime is around 1 μs. As expected, it passes close to the maximum magnetic field effect. Figure 4c also shows the predicted rate constants for RP_C and a composite radical pair—as in Fig. 4b, but with the values of $\langle k_f \rangle$ scaled down by a factor of 10. Such a change in the average rate constant of the forward reaction would optimize the predicted magnetic field effect for the

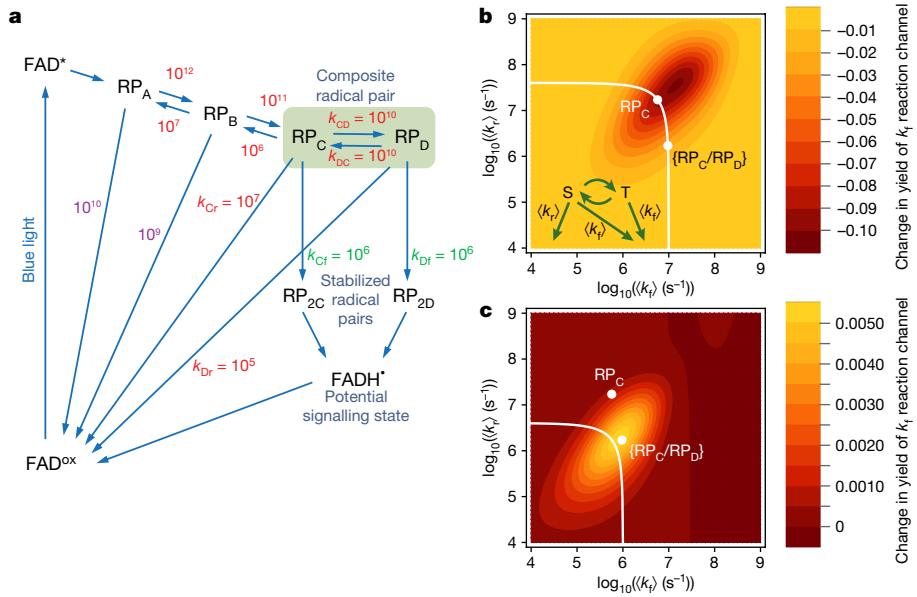

Fig. 4 | Reaction scheme and simulated magnetic field effects for *Er*CRY4. **a**, Proposed reaction scheme for magnetic sensing and signalling by CRY4 in night-migratory songbirds. The arrows are labelled with approximate rate constants (in s^{-1}): red, calculations based on molecular dynamics simulations; purple, transient absorption measurements; green, estimated from magnetic field effects. **b**, Spin dynamics simulation for the reaction scheme shown at the bottom left, in which the curved arrows represent the coherent interconversion of the singlet (S) and triplet (T) states of a composite radical pair and the straight arrows indicate the competing reaction pathways. $\langle k_f \rangle$ and $\langle k_r \rangle$ are weighted averages of the corresponding rate constants for RP_C and RP_D. The contour plot shows the change in the yield of the $\langle k_f \rangle$ pathway caused by a 30-mT magnetic field as a function of $\langle k_f \rangle$ and $\langle k_r \rangle$. On the white line the lifetime of the composite radical pair is approximately 100 ns. The positions of the white spots correspond to the rate constants estimated for RP_C and the composite pair with $f_C = 0.1$. See Supplementary Information for details. **c**, As **b**, except that the magnetic field is 50 μT and the white line corresponds to a lifetime of the composite radical pair of approximately 1 μs. The white spots have been moved −1.0 log units along the $\langle k_f \rangle$ axis.

composite radical pair and cause it to outperform RP_C in a 50-μT field. A reduction in $\langle k_f \rangle$ of this magnitude could be achieved in vivo by a combination of smaller changes in the individual forward rate constants for RP_C and RP_D (k_{Cf} and k_{Df}) and the equilibrium proportions of the two radical pairs (f_C). Small changes in the two recombination rates (k_{Cr} and k_{Dr}) might also be advantageous. Such variations could arise from protein–protein interactions that reduced the solvent accessibility of the two $TrpH^{\bullet+}$ radicals (and slowed their deprotonation) and produced small shifts in the position of the RP_C/RP_D equilibrium. It is anticipated that a viable cryptochrome magnetoreceptor would require protein interaction partners in vivo both for signalling and to restrict its orientational freedom (as some degree of immobilization is required for directional sensing[43]). Protein–protein interactions could also enhance the sensitivity to magnetic fields of around 50 μT in vivo by restricting the internal mobility of the radicals and so reducing the effect of spin relaxation[40,44]. CRY4 molecules are not expected to show substantial responses to Earth-strength magnetic fields in vitro unless they are anchored, aligned and associated with the appropriate signalling partners. None of the proteins required for these interactions is currently known (but see ref. [45]). Furthermore, magnetic sensitivity could be enhanced by receptor alignment[41], biochemical amplification[45] and neural processing[3]. These aspects can also be optimized by evolution and could substantially improve the magnetic sensitivity of the robin's magnetic sense.

In conclusion, we have demonstrated that CRY4 from the night-migratory European robin seems to be fit for purpose as a magnetic sensor, and that it is more magnetically sensitive than CRY4 from the non-migratory pigeon and chicken under identical measurement conditions in vitro. Our data also suggest that nature might have found ways to independently optimize the magnetic sensing and signalling properties of CRY4 through control of its photochemistry. To determine whether CRY4 acts as a magnetoreceptor molecule in vivo, direct manipulations of this protein in the eyes of night-migratory songbirds would be required. We hope that such experiments will become possible in the future.

Online content

Any methods, additional references, Nature Research reporting summaries, source data, extended data, supplementary information, acknowledgements, peer review information; details of author contributions and competing interests; and statements of data and code availability are available at https://doi.org/10.1038/s41586-021-03618-9.

1. Mouritsen, H. Long-distance navigation and magnetoreception in migratory animals. *Nature* **558**, 50–59 (2018).
2. Wiltschko, W., Munro, U., Ford, H. & Wiltschko, R. Red-light disrupts magnetic orientation of migratory birds. *Nature* **364**, 525–527 (1993).
3. Zapka, M. et al. Visual but not trigeminal mediation of magnetic compass information in a migratory bird. *Nature* **461**, 1274–1277 (2009).
4. Hore, P. J. & Mouritsen, H. The radical-pair mechanism of magnetoreception. *Annu. Rev. Biophys.* **45**, 299–344 (2016).
5. Ritz, T., Adem, S. & Schulten, K. A model for photoreceptor-based magnetoreception in birds. *Biophys. J.* **78**, 707–718 (2000).
6. Ritz, T., Thalau, P., Phillips, J. B., Wiltschko, R. & Wiltschko, W. Resonance effects indicate a radical-pair mechanism for avian magnetic compass. *Nature* **429**, 177–180 (2004).
7. Engels, S. et al. Anthropogenic electromagnetic noise disrupts magnetic compass orientation in a migratory bird. *Nature* **509**, 353–356 (2014).
8. Steiner, U. E. & Ulrich, T. Magnetic field effects in chemical kinetics and related phenomena. *Chem. Rev.* **89**, 51–147 (1989).
9. Maeda, K. et al. Chemical compass model of avian magnetoreception. *Nature* **453**, 387–390 (2008).
10. Kerpal, C. et al. Chemical compass behaviour at microtesla magnetic fields strengthens the radical pair hypothesis of avian magnetoreception. *Nat. Commun.* **10**, 3707 (2019).
11. Giovani, B., Byrdin, M., Ahmad, M. & Brettel, K. Light-induced electron transfer in a cryptochrome blue-light photoreceptor. *Nat. Struct. Biol.* **10**, 489–490 (2003).
12. Müller, P., Yamamoto, J., Martin, R., Iwai, S. & Brettel, K. Discovery and functional analysis of a 4th electron-transferring tryptophan conserved exclusively in animal cryptochromes and (6-4) photolyases. *Chem. Commun.* **51**, 15502–15505 (2015).
13. Nohr, D. et al. Determination of radical–radical distances in light-active proteins and their implication for biological magnetoreception. *Angew. Chem. Int. Ed.* **56**, 8550–8554 (2017).

14. Nohr, D. et al. Extended electron-transfer pathways in animal cryptochromes mediated by a tetrad of aromatic amino acids. *Biophys. J.* **111**, 301–311 (2016).
15. Zoltowski, B. D. et al. Chemical and structural analysis of a photoactive vertebrate cryptochrome from pigeon. *Proc. Natl Acad. Sci. USA* **116**, 19449–19457 (2019).
16. Sheppard, D. M. W. et al. Millitesla magnetic field effects on the photocycle of an animal cryptochrome. *Sci. Rep.* **7**, 42228 (2017).
17. Maeda, K. et al. Magnetically sensitive light-induced reactions in cryptochrome are consistent with its proposed role as a magnetoreceptor. *Proc. Natl Acad. Sci. USA* **109**, 4774–4779 (2012).
18. Fedele, G., Green, E. W., Rosato, E. & Kyriacou, C. P. An electromagnetic field disrupts negative geotaxis in *Drosophila* via a CRY-dependent pathway. *Nat. Commun.* **5**, 4391 (2014).
19. Gegear, R. J., Casselman, A., Waddell, S. & Reppert, S. M. Cryptochrome mediates light-dependent magnetosensitivity in *Drosophila*. *Nature* **454**, 1014–1018 (2008).
20. Hoang, N. et al. Human and *Drosophila* cryptochromes are light activated by flavin photoreduction in living cells. *PLoS Biol.* **6**, e160 (2008).
21. Pooam, M. et al. Magnetic sensitivity mediated by the *Arabidopsis* blue-light receptor cryptochrome occurs during flavin reoxidation in the dark. *Planta* **249**, 319–332 (2019).
22. Xu, C. X., Lv, Y., Chen, C. F., Zhang, Y. X. & Wei, S. F. Blue light-dependent phosphorylations of cryptochromes are affected by magnetic fields in *Arabidopsis*. *Adv. Space Res.* **53**, 1118–1124 (2014).
23. Giachello, C. N. G., Scrutton, N. S., Jones, A. R. & Baines, R. A. Magnetic fields modulate blue-light-dependent regulation of neuronal firing by cryptochrome. *J. Neurosci.* **36**, 10742–10749 (2016).
24. Watari, R. et al. Light-dependent structural change of chicken retinal cryptochrome4. *J. Biol. Chem.* **287**, 42634–42641 (2012).
25. Günther, A. et al. Double-cone localization and seasonal expression pattern suggest a role in magnetoreception for European robin cryptochrome 4. *Curr. Biol.* **28**, 211–223.e4 (2018).
26. Nießner, C., Denzau, S., Peichl, L., Wiltschko, W. & Wiltschko, R. Magnetoreception in birds: I. Immunohistochemical studies concerning the cryptochrome cycle. *J. Exp. Biol.* **217**, 4221–4224 (2014).
27. Nießner, C., Denzau, S., Peichl, L., Wiltschko, W. & Wiltschko, R. Magnetoreception: activation of avian cryptochrome 1a in various light conditions. *J. Comp. Physiol. A* **204**, 977–984 (2018).
28. Wiltschko, R., Ahmad, M., Nießner, C., Gehring, D. & Wiltschko, W. Light-dependent magnetoreception in birds: the crucial step occurs in the dark. *J. R. Soc. Interface* **13**, 20151010 (2016).
29. Player, T. C. & Hore, P. J. Viability of superoxide-containing radical pairs as magnetoreceptors. *J. Chem. Phys.* **151**, 225101 (2019).
30. Müller, P. & Ahmad, M. Light-activated cryptochrome reacts with molecular oxygen to form a flavin–superoxide radical pair consistent with magnetoreception. *J. Biol. Chem.* **286**, 21033–21040 (2011).
31. Bolte, P. et al. Cryptochrome 1a localisation in light- and dark-adapted retinae of several migratory and non-migratory bird species: no signs of light-dependent activation. *Ethol. Ecol. Evol.* https://doi.org/10.1080/03949370.2020.1870571 (2021).
32. Kutta, R. J., Archipowa, N., Johannissen, L. O., Jones, A. R. & Scrutton, N. S. Vertebrate cryptochromes are vestigial flavoproteins. *Sci. Rep.* **7**, 44906 (2017).
33. Qin, S. et al. A magnetic protein biocompass. *Nat. Mater.* **15**, 217–226 (2016).
34. Maeda, K. et al. Following radical pair reactions in solution: a step change in sensitivity using cavity ring-down detection. *J. Am. Chem. Soc.* **133**, 17807–17815 (2011).
35. Neil, S. R. T. et al. Broadband cavity-enhanced detection of magnetic field effects in chemical models of a cryptochrome magnetoreceptor. *J. Phys. Chem. B* **118**, 4177–4184 (2014).
36. Roos, A. & Boron, W. F. Intracellular pH. *Physiol. Rev.* **61**, 296–434 (1981).
37. Reeves, R. B. The interaction of body temperature and acid–base balance in ectothermic vertebrates. *Annu. Rev. Physiol.* **39**, 559–586 (1977).
38. Weber, S. et al. Origin of light-induced spin-correlated radical pairs in cryptochrome. *J. Phys. Chem. B* **114**, 14745–14754 (2010).
39. Hochstoeger, T. et al. The biophysical, molecular, and anatomical landscape of pigeon CRY4: a candidate light-based quantal magnetosensor. *Sci. Adv.* **6**, eabb9110 (2020).
40. Kattnig, D. R., Solov'yov, I. A. & Hore, P. J. Electron spin relaxation in cryptochrome-based magnetoreception. *Phys. Chem. Chem. Phys.* **18**, 12443–12456 (2016).
41. Efimova, O. & Hore, P. J. Role of exchange and dipolar interactions in the radical pair model of the avian magnetic compass. *Biophys. J.* **94**, 1565–1574 (2008).
42. Timmel, C. R., Till, U., Brocklehurst, B., McLauchlan, K. A. & Hore, P. J. Effects of weak magnetic fields on free radical recombination reactions. *Mol. Phys.* **95**, 71–89 (1998).
43. Worster, S., Mouritsen, H. & Hore, P. J. A light-dependent magnetoreception mechanism insensitive to light intensity and polarization. *J. R. Soc. Interface* **14**, 20170405 (2017).
44. Kattnig, D. R., Sowa, J. K., Solov'yov, I. A. & Hore, P. J. Electron spin relaxation can enhance the performance of a cryptochrome-based magnetic compass sensor. *New J. Phys.* **18**, 063007 (2016).
45. Wu, H., Scholten, A., Einwich, A., Mouritsen, H. & Koch, K. W. Protein–protein interaction of the putative magnetoreceptor cryptochrome 4 expressed in the avian retina. *Sci. Rep.* **10**, 7364 (2020).

Reporting summary

Further information on research design is available in the Nature Research Reporting Summary linked to this paper.

Data availability

The complete set of molecular dynamics simulation and quantum chemistry data (300 GB) can be downloaded from the University of Oldenburg repository: https://cloud.uol.de/s/NrTYpoEzL6RbPq7. Specific molecular dynamics data can also be obtained directly from I.A.S. on request. Source data are provided with this paper.

Acknowledgements This work was supported by the Air Force Office of Scientific Research (Air Force Materiel Command, USAF award no. FA9550-14-1-0095, to P.J.H., H.M., C.R.T., S.R.M. and K.-W.K.); by the European Research Council (under the European Union's Horizon 2020 research and innovation programme, grant agreement no. 810002, Synergy Grant: 'QuantumBirds', awarded to P.J.H. and H.M.); by the Office of Naval Research Global, award no. N62909-19-1-2045, to P.J.H., C.R.T. and S.R.M.; by the Deutsche Forschungsgemeinschaft (SFB 1372, 'Magnetoreception and navigation in vertebrates', project number: 395940726 to H.M., K.-W.K., I.A.S. and P.J.H., and GRK 1885, 'Molecular basis of sensory biology' to K.-W.K., I.A.S. and H.M.); by a DAAD (German Academic Exchange Service, Graduate School Scholarship Programme, ID 57395813) stipend to J.X.; by funding for G.M. from the SCG Innovation Fund; by the Electromagnetic Fields Biological Research Trust (to P.J.H., C.R.T. and S.R.M.); by the National Natural Science Foundation of China, grant no. 31640001, and the Presidential Foundation of Hefei Institutes of Physical Science, Chinese Academy of Sciences, grant no. BJZX201901 (to C.X.); and by the Lundbeck Foundation, the Danish Councils for Independent Research, and the Volkswagen Foundation (to I.A.S.). V.D. is grateful to the Clarendon Fund, University of Oxford. M.J.G. thanks the Biotechnology and Biological Sciences Research Council, grant number BB/M011224/1 and the Clarendon Fund. We acknowledge use of the Advanced Research Computing (ARC) facility of the University of Oxford. J.S.T. is an Investigator and Y.C. is a Research Specialist in the Howard Hughes Medical Institute. I.A.S. is grateful to the DeiC National HPC Center, University of Southern Denmark for computational resources. We thank B. Grünberg, I. Fomins, A. Günther and A. Einwich for laboratory assistance and for providing protein sequence information. J.X. thanks Y. Tan for training in protein expression and purification. We thank S. Chandler for mass spectrometry, S. Y. Wong for assistance with spin dynamics calculations, and W. Myers (CAESR, Engineering and Physical Sciences Research Council, grant no. EP/L011972/1) for obtaining a threefold improvement in the time-resolved electron paramagnetic resonance signal. We are grateful to the staff of the mechanical and electronic workshops in the Oxford Chemistry Department and at the University of Oldenburg.

Author contributions J.X., L.E.J., T.Z., M.K., K.B.H., S.R. and M.J.G. made particularly important experimental contributions. J.X. cloned wild-type *Er*CRY4 and all the mutants and developed the protocols for expression and purification of the proteins with FAD bound. J.X. and J.S. produced the protein samples. L.E.J. developed the continuous illumination experiment for studying photoreduction and the picosecond transient absorption experiment for measuring magnetic field effects, and recorded and interpreted data. T.Z. and M.J.G. developed the CRDS experiment for measuring magnetic field effects and recorded and interpreted data. M.K. developed the broadband cavity-enhanced absorption spectroscopy experiment for measuring magnetic field effects and recorded and interpreted data. S.R. and S.W. recorded and interpreted the EPR data. K.B.H. participated in all five of the above experiments and recorded and interpreted spectroscopic data. J.F., with K.B.H., recorded and interpreted some of the transient absorption data and all of the re-oxidation data. M.K. helped with the global analysis of the re-oxidation data. M.J.G., V.D., J.R.W. and P.D.F.M. made spectroscopic measurements of magnetic field effects. D.J.C.S. helped to develop the picosecond TA apparatus. J.L. and Y.W. performed spin dynamics calculations. T.L.P. and G.M. reproduced and helped to interpret the EPR data. A.S.G. recorded and interpreted mass spectra. M.B. expressed and purified chicken CRY4. M.H., S.H., G.D. and S.J.K. expressed and purified some of the *Er*CRY4 protein samples. Y.C., J.S.T. and J.X. expressed and purified pigeon CRY4. H.Y., H.W., K.-W.K., R.B. and C.X. provided advice on protein expression. I.A.S. performed molecular dynamics simulations and provided advice on cryptochrome structure and dynamics. L.E.J. had oversight of the organization and administration of the optical spectroscopy measurements. P.J.H., H.M., C.R.T. and S.R.M. conceived the study. P.J.H., H.M., C.R.T., S.R.M. and C.X. supervised the work. P.J.H. and H.M. wrote the manuscript, and all authors commented on the manuscript.

Competing interests The authors declare no competing interests.

Additional information

Supplementary information The online version contains supplementary material available at https://doi.org/10.1038/s41586-021-03618-9.

Correspondence and requests for materials should be addressed to I.A.S., C.X., S.R.M., C.R.T., H.M. or P.J.H.

Peer review information *Nature* thanks Aurelien de la Lande, Thorsten Ritz, Eric Warrant and the other, anonymous, reviewer(s) for their contribution to the peer review of this work.

nature research

Corresponding author(s): P. J. Hore and H. Mouritsen

Last updated by author(s): Apr 10, 2021

Reporting Summary

Nature Research wishes to improve the reproducibility of the work that we publish. This form provides structure for consistency and transparency in reporting. For further information on Nature Research policies, see Authors & Referees and the Editorial Policy Checklist.

Statistics

For all statistical analyses, confirm that the following items are present in the figure legend, table legend, main text, or Methods section.

n/a	Confirmed	
☐	☒	The exact sample size (*n*) for each experimental group/condition, given as a discrete number and unit of measurement
☐	☒	A statement on whether measurements were taken from distinct samples or whether the same sample was measured repeatedly
☒	☐	The statistical test(s) used AND whether they are one- or two-sided *Only common tests should be described solely by name; describe more complex techniques in the Methods section.*
☒	☐	A description of all covariates tested
☒	☐	A description of any assumptions or corrections, such as tests of normality and adjustment for multiple comparisons
☐	☒	A full description of the statistical parameters including central tendency (e.g. means) or other basic estimates (e.g. regression coefficient) AND variation (e.g. standard deviation) or associated estimates of uncertainty (e.g. confidence intervals)
☒	☐	For null hypothesis testing, the test statistic (e.g. *F*, *t*, *r*) with confidence intervals, effect sizes, degrees of freedom and *P* value noted *Give P values as exact values whenever suitable.*
☒	☐	For Bayesian analysis, information on the choice of priors and Markov chain Monte Carlo settings
☒	☐	For hierarchical and complex designs, identification of the appropriate level for tests and full reporting of outcomes
☒	☐	Estimates of effect sizes (e.g. Cohen's *d*, Pearson's *r*), indicating how they were calculated

Our web collection on statistics for biologists contains articles on many of the points above.

Software and code

Policy information about availability of computer code

Data collection	The custom codes used to generate the contour plots in Fig. 4b and c and the simulations in Fig. S4 (both Wolfram Mathematica 12) can be downloaded from: http://hore.chem.ox.ac.uk/Nature_2021/Codes.zip. The custom codes written to control and acquire data from our home-built magnetic field effect spectrometers (LabView v.15 and C++) are available from PJH on request. Given that these instruments are unique, the control software is unlikely to be of use to anyone else which is why they are not made publicly available. NAMD 2.10 (http://www.ks.uiuc.edu/Research/namd/) and VIKING (https://viking-suite.com/) were used for the molecular dynamics simulations. All relevant input and output files for the molecular dynamics simulations are available for download from the University of Oldenburg repository: https://cloud.uol.de/s/NrTYpoEzL6RbPq7.
Data analysis	VMD 1.9.3 (http://www.ks.uiuc.edu/Research/vmd/) was used for analysis of molecular dynamics data. UNICORN, GE Healthcare, versions 7.1 and 7.3, control software for chromatography. The ShakeH algorithm is a standard component of NAMD.

For manuscripts utilizing custom algorithms or software that are central to the research but not yet described in published literature, software must be made available to editors/reviewers. We strongly encourage code deposition in a community repository (e.g. GitHub). See the Nature Research guidelines for submitting code & software for further information.

Data

Policy information about availability of data

All manuscripts must include a data availability statement. This statement should provide the following information, where applicable:

- Accession codes, unique identifiers, or web links for publicly available datasets
- A list of figures that have associated raw data
- A description of any restrictions on data availability

All relevant spectroscopic data are presented in Figures in the manuscript or in the Supplementary Information. The data used to prepare the figures are available as Supplementary Data files.

The complete set of molecular dynamics simulation data is available for download from the University of Oldenburg repository: https://cloud.uol.de/s/NrTYpoEzL6RbPq7. Specific molecular dynamics data can also be obtained directly from IAS on request.

Field-specific reporting

Please select the one below that is the best fit for your research. If you are not sure, read the appropriate sections before making your selection.

☒ Life sciences ☐ Behavioural & social sciences ☐ Ecological, evolutionary & environmental sciences

For a reference copy of the document with all sections, see nature.com/documents/nr-reporting-summary-flat.pdf

Life sciences study design

All studies must disclose on these points even when the disclosure is negative.

Sample size	All experimental data were spectroscopic measurements on samples of proteins. Measurements were repeated and the signals averaged until the signal-to-noise ratio was judged satisfactory. The number of measurements on each sample depended on the particular instrument used and the strength of the signals. Detailed information is provided in the Statistics & Reproducibility subsection in the Methods section.
Data exclusions	Occasional spectroscopic measurements failed to yield usable data as a result of instrument breakdowns, protein precipitation, etc.
Replication	The number of repeats of each measurement using independently produced batches of protein is given in the Statistics & Reproducibility subsection in the Methods section.
Randomization	Not relevant for spectroscopic measurements.
Blinding	Blinding is not appropriate for the spectroscopic measurements reported here. No stastistical tests were required to interpret the results.

Reporting for specific materials, systems and methods

We require information from authors about some types of materials, experimental systems and methods used in many studies. Here, indicate whether each material, system or method listed is relevant to your study. If you are not sure if a list item applies to your research, read the appropriate section before selecting a response.

Materials & experimental systems

n/a	Involved in the study
☒	☐ Antibodies
☒	☐ Eukaryotic cell lines
☒	☐ Palaeontology
☒	☐ Animals and other organisms
☒	☐ Human research participants
☒	☐ Clinical data

Methods

n/a	Involved in the study
☒	☐ ChIP-seq
☒	☐ Flow cytometry
☒	☐ MRI-based neuroimaging